


## NEUROSYSTEMS

# Mirror trends of plasticity and stability indicators in primate prefrontal cortex

Miguel Á. García-Cabezas,<sup>1</sup> Mary Kate P. Joyce,<sup>1</sup> Yohan J. John,<sup>1</sup> Basilis Zikopoulos<sup>2</sup> and Helen Barbas<sup>1</sup> <sup>1</sup>Neural Systems Laboratory, Department of Health Sciences, Boston University, 635 Commonwealth Ave, Boston, MA 02215, USA<sup>2</sup>Human Systems Neuroscience Laboratory, Boston University, Boston, MA, USA**Keywords:** eulamine, limbic, macaque monkey, plasticity, selective vulnerability

## Abstract

Research on plasticity markers in the cerebral cortex has largely focused on their timing of expression and role in shaping circuits during critical and normal periods. By contrast, little attention has been focused on the spatial dimension of plasticity–stability across cortical areas. The rationale for this analysis is based on the systematic variation in cortical structure that parallels functional specialization and raises the possibility of varying levels of plasticity. Here, we investigated in adult rhesus monkeys the expression of markers related to synaptic plasticity or stability in prefrontal limbic and eulamine areas that vary in laminar structure. Our findings revealed that limbic areas are impoverished in three markers of stability: intracortical myelin, the lectin *Wisteria floribunda* agglutinin, which labels perineuronal nets, and parvalbumin, which is expressed in a class of strong inhibitory neurons. By contrast, prefrontal limbic areas were enriched in the enzyme calcium/calmodulin-dependent protein kinase II (CaMKII), known to enhance plasticity. Eulamine areas have more elaborate laminar architecture than limbic areas and showed the opposite trend: they were enriched in markers of stability and had lower expression of the plasticity-related marker CaMKII. The expression of glial fibrillary acidic protein (GFAP), a marker of activated astrocytes, was also higher in limbic areas, suggesting that cellular stress correlates with the rate of circuit reshaping. Elevated markers of plasticity may endow limbic areas with flexibility necessary for learning and memory within an affective context, but may also render them vulnerable to abnormal structural changes, as seen in neurologic and psychiatric diseases.

## Introduction

Plasticity is the property of neural circuits to reshape their connectivity by experience to achieve novel functions (Paillard, 1976; Will *et al.*, 2008; Berlucchi & Buchtel, 2009). In the adult cerebral cortex, the best studied mechanisms for circuit reshaping require structural modification of synapses at two levels. The first level involves changes in the strength of existing excitatory synapses by modification of postsynaptic receptors that result in long-term potentiation (LTP) or long-term depression (LTD; Lisman *et al.*, 2012; Cooke & Bear, 2014; Shipton & Paulsen, 2014; Lisman, 2017). The second level involves disassembling old synapses and forming new synapses with participation of axon terminals and dendritic spines

(Gogolla *et al.*, 2007; Holtmaat & Svoboda, 2009; Holtmaat *et al.*, 2013). Higher rate of disassembly and formation of synapses during postnatal critical periods is followed by circuit stabilization during adult normal periods (Nabel & Morishita, 2013; Takesian & Hensch, 2013).

There is a dearth of studies that compare synaptic plasticity in a spatial dimension across brain regions during normal periods. This is particularly striking for the cerebral cortex, which is a heterogeneous structure characterized by systematic variation across areas [reviewed in Barbas (2015)]. For example, cortical lamination is least differentiated in cortical limbic areas and is increasingly more elaborate along a series of six-layered (eulamine) areas. Other architectonic and cellular features, like myelin content and spine density of pyramidal excitatory neurons, also vary systematically across areas in gradients that parallel laminar elaboration (Sanides, 1970; Barbas & Pandya, 1987, 1989; Nieuwenhuys, 2013; Elston & Fujita, 2014; Barbas & García-Cabezas, 2015; Medalla & Luebke, 2015; Medalla *et al.*, 2017). Plasticity in the adult cortex was suspected to be higher in limbic areas based on cellular features (Barbas, 1995), which was subsequently supported by findings that in adult primates anterior cingulate (limbic) areas have higher capacity for spine and synapse formation than dorsolateral (eulamine) prefrontal areas (Sasaki *et al.*, 2015).

Correspondence: Helen Barbas, as above.

E-mail: barbas@bu.edu

Received 7 April 2017, revised 22 August 2017, accepted 24 August 2017

Edited by Patricia Gaspar

Reviewed by Tommaso Pizzorusso, Institute of Neuroscience, National Research Council, Italy; and Guy Elston, Centre for Cognitive Neuroscience, Sunshine Coast, Australia

The associated peer review process communications can be found in the online version of this article.

Here, we systematically investigated cellular and molecular markers that either enhance or limit synaptic plasticity in limbic and eulaminar prefrontal areas that vary in laminar structure. Specifically, we studied three markers known to limit plasticity: the first was parvalbumin (PV) expressed in some inhibitory neurons, whose activation helps end critical periods and limits LTP and LTD in adult cortex (Saez & Friedlander, 2016). The second was the lectin *Wisteria floribunda* agglutinin (WFA), a marker of perineuronal nets (PNNs) reported to surround PV inhibitory neurons (Hartig *et al.*, 1992, 1994). Chemical removal of PNNs in the cortex restores plasticity to the level of the critical period (Pizzorusso *et al.*, 2002; Sorg *et al.*, 2016; Lensjo *et al.*, 2017). The third marker was intracortical myelin, which is also associated with ending critical periods and reducing spine turnover and LTP in the cortex (Akbik *et al.*, 2012; Schwab & Strittmatter, 2014; Boghdadi *et al.*, 2017). The second group of markers, with presumed opposite expression, included the enzyme CaMKII, because of its key role in mediating LTP (Lisman *et al.*, 2012; Colgan & Yasuda, 2014). We also examined two glial markers: the glial fibrillary acidic protein (GFAP), which labels activated and reactive astrocytes and is an indicator of cellular stress (Sofroniew & Vinters, 2010; Hol & Pekny, 2015), and the ionized calcium binding adapter molecule 1 (Iba1), which is specific for microglia (Ito *et al.*, 1998; Torres-Platas *et al.*, 2014). The Iba1 is a good marker for resting microglia in nonpathological states (Hendrickx *et al.*, 2017).

Our findings revealed that limbic areas are enriched in markers that enable plasticity, but are impoverished in markers that underlie stability, while eulaminar areas show the opposite trend. High expression of plasticity markers in limbic areas may facilitate engagement in emotions and memory, but may also account for their increased vulnerability to psychiatric and neurologic diseases (Arnold *et al.*, 1991; Mayberg *et al.*, 2005; Zikopoulos & Barbas, 2010).

## Methods and materials

### *Animal cases, perfusion and tissue processing*

We obtained data from prefrontal cortex of 11 young adult rhesus monkeys (*Macaca mulatta*). Detailed protocols were approved by Institutional Animal Care and Use Committees (Harvard Medical School and Boston University School of Medicine) according to NIH guidelines [DHEW Publication no. (NIH) 80-22, revised 1996, Bethesda, MD, USA].

Animals were deeply anaesthetized with a lethal dose of sodium pentobarbital (~50 mg/kg, intravenous, to effect) and perfused transcardially, with either 4% paraformaldehyde in cacodylate buffer or PBS (0.1 M, pH 7.4; cases AL, AN, AQ, AS, AT, AV, AZ, BB and BD), or saline followed by 6% paraformaldehyde in PB, 0.1 M, pH 7.4 (cases AJ and AK). These cases were also used for other studies (Barbas, 1993; Dombrowski & Barbas, 1996; Zikopoulos & Barbas, 2006; Ghashghaei *et al.*, 2007; García-Cabezas & Barbas, 2017). Brains were removed from the skull, photographed, cryoprotected in ascending sucrose solutions (10–30% in PBS 0.01 M at pH 7.4), frozen in –75 °C isopentane (Fisher Scientific, Pittsburgh, PA, USA) for rapid and uniform freezing (Rosene *et al.*, 1986) and cut in the coronal plane on a freezing microtome at 40 or 50 µm to produce 10 matched series.

### *Assays and stains*

To estimate neuron, astrocyte and microglia density, we stained series of sections for Nissl ( $n = 3$  cases) which stains all neurons and glia and allows their distinction (García-Cabezas *et al.*, 2016).

Intracortical myelin was stained in series of sections using the Gallyas silver technique [ $n = 5$  cases; Gallyas (1979); Zikopoulos *et al.* (2016)]. We employed immunohistochemical methods to label PV ( $n = 3$  cases), which labels a neurochemical and functionally distinct class of inhibitory neurons in primate cerebral cortex (DeFelipe, 1997), WFA ( $n = 2$  cases), which recognizes *N*-acetylgalactosamine-containing epitopes in the CS-GAG chains and labels extracellular PNNs (Hartig *et al.*, 1992, 1994),  $\alpha$ CaMKII ( $n = 2$  cases), GFAP ( $n = 2$  cases) and Iba1 ( $n = 2$  cases). Briefly, free-floating sections were rinsed in PBS (0.01 M, pH 7.4), incubated in 0.01 M sodium citrate buffer, pH 8.5, at 80–85 °C for 30 min for antigen retrieval (only for WFA staining), incubated for 1 h in 0.05 M glycine and pre-blocked [10% normal goat or horse serum, 5% bovine serum albumin (BSA) and 0.2% Triton X-100 in PBS]. Sections were then incubated overnight in WFA (Biotinylated *Wisteria floribunda* lectin, cat. no. B-1355, Vector Laboratories, Burlingame, CA, USA; diluted 1/200) or in primary antibody against PV (mouse anti-PV, cat. no. 235, Swant Antibodies, Marly, Switzerland; diluted 1 : 3000),  $\alpha$ CaMKII (mouse anti- $\alpha$ CaMKII, cat. no. 1481703, Boehringer Mannheim, Indianapolis, IN, USA; diluted 1 : 400), GFAP (rabbit anti-GFAP, cat. no. G9269, Sigma-Aldrich, St. Louis, MO, USA; diluted 1 : 500) or Iba1 (goat anti-Iba1, cat. no. ab5076, Abcam, Cambridge, MA, USA; diluted 1 : 1000 in PBS, 1% normal goat or horse serum, 1% BSA and 0.1% Triton X-100), rinsed in PBS and incubated for 4 h in the respective secondary biotinylated antibody (goat anti-mouse IgG, cat. no. BA-9200; goat anti-rabbit IgG, cat. no. BA-1000; horse anti-mouse IgG, cat. no. BA-2000; or horse anti-goat, BA-9500; Vector Laboratories, diluted 1 : 200 in PBS, 1% normal goat or horse serum, 1% BSA and 0.1% Triton X-100). For biotinylated WFA, no secondary antibody was needed. We then incubated sections for 1 h in avidin–biotin horseradish peroxidase complex (AB-HRP kit; Vectastain PK-6100 ABC Elite kit, Vector Laboratories; diluted 1 : 100 in 0.01 M PBS with 0.1% Triton X-100), rinsed in PBS and processed for 2–3 min for the peroxidase-catalysed polymerization of diaminobenzidine (DAB; Vector or Zymed Laboratories Inc., South San Francisco, CA, USA; 0.05% DAB and 0.004% H<sub>2</sub>O<sub>2</sub> in PBS). Sections were mounted on gelatin-coated slides and dried, and some were counterstained for Nissl (García-Cabezas *et al.*, 2016), dehydrated in graded alcohols, cleared in xylenes and coverslipped with mounting media (Permount, Fisher Scientific; or Entellan, EM Sciences, Hatfield, PA, USA).

### *Unbiased estimate of PV and Nissl-stained neurons, astrocytes and microglia*

We estimated the density of parvalbumin-positive (PV+) neurons, their proportion in the entire neuron population and the density of astrocytes and microglia. Measures were obtained from representative columns along the depth of the gyrus part of anterior cingulate areas 25 and 32, medial area 10 (10m) and caudal dorsolateral area 46d (Fig. 1), based on the maps of Barbas & Pandya (1989). We used the unbiased stereological method of the optical fractionator (Gundersen, 1986; Howard & Reed, 1998) in conjunction with a commercial system (StereoInvestigator; MicroBrightField, Inc., Williston VT, USA), as described [e.g. García-Cabezas & Barbas (2014a,b)]. We first drew contours of layers in each column (layers I and II–III in all areas; layers IV–VI in areas 25 and 32; layers IV and V–VI in eulaminar areas 10m and 46d) to estimate the number of neurons, astrocytes and microglia by laminar groups or for entire columns (I–VI). We counted PV+ neurons at 400 $\times$  and Nissl-stained neurons, astrocytes and microglia at 1000 $\times$  from a minimum

FIG. 1. Limbic and eulaminar areas of the monkey prefrontal cortex differ in laminar structure. (A, B) Maps of monkey prefrontal cortex (Barbas & Pandya, 1989). (A) Medial surface; (B) lateral surface. The maps show areas with the lowest (black) and highest (lightest grey) laminar elaboration. (C–F) Photomicrographs of areas 25, 32, 10m and 46d stained with Nissl. (C, D) Areas 25 and 32 have a rudimentary layer IV (dysgranular). Layer I is thick and shows poor delimitation with layer II. Deep layers V–VI are more prominent than superficial layers II–III. (E) Eulaminar (I) area 10m has six layers. (F) Layer IV in eulaminar (II) area 46d is better developed than in area 10m. Layer I is thinner than in areas 25 and 32 and is delineated from layer II. Superficial layers II–III are denser than in limbic areas 25 and 32. MPAll, medial periallocortex; WM, white matter. Arabic numerals show cortical areas according to Barbas & Pandya (1989). Roman numerals indicate cortical layers. Calibration bar in F applies to C–F. [Colour figure can be viewed at [wileyonlinelibrary.com](http://wileyonlinelibrary.com)].

of three evenly spaced sections/case/area, using systematic random sampling. The counting frame (dissector) size for PV+ neurons was 200  $\mu\text{m}$ , and for neuron, astrocyte and microglia counts, it was 50–60  $\mu\text{m}$ , based on pilot study. We used as guard zones the top and bottom of each section (minimum 2  $\mu\text{m}$  in 10- to 15- $\mu\text{m}$  sections after tissue shrinkage). We measured section thickness at each counting site using the software program. The height of the counting frame was 5  $\mu\text{m}$  and grid spacing was 100–300  $\mu\text{m}$ . Neurons, astrocytes and microglia were counted if their nuclei fell within the counting frame or touched the two acceptance lines but not the two forbidden lines (Howard & Reed, 1998). These parameters yielded a sampling fraction with a coefficient of error of < 10% per contour, with the exception of PV+ neurons in layer IV where the error was < 15%, due to the small laminar volume, as recommended (Gundersen, 1986; Howard & Reed, 1998). We computed cell density by dividing the estimated number of counted cells with the estimated volume of each contour.

#### Optical density analysis of intracortical myelin, WFA, $\alpha\text{CaMKII}$ and GFAP

We quantified intracortical myelin content, WFA,  $\alpha\text{CaMKII}$  or GFAP expression using optical density from photomicrographs of representative columns from each area. We first captured images under bright field (myelin, WFA and  $\alpha\text{CaMKII}$ ) or dark field (GFAP) with a CCD camera (Olympus DP70) mounted on an optical microscope (Olympus BX 51) connected to a personal computer using image software (DP Controller). We captured images at 100 $\times$  (UPlanFl 10 $\times$ /0.30 Japan) with the same light exposure and obtained optical density measurements from 5 to 15 images taken from 3 to 8 sections per marker/case/area.

We imported photographs into MATLAB (MATLAB and Statistics Toolbox Release R2015b, The MathWorks, Inc., Natick, MA, USA) to convert into grey scale. Each bright-field image was inverted by subtracting pixel values from the darkest possible pixel value, so that pixels with strong staining had higher numerical values than the background. We measured the mean grey level density for each image and obtained overall mean grey level values for each area. We then estimated the grey level density along the depth of normalized columns, encompassing cortical thickness from the pial surface to the white matter. This involved two steps for each image: first, we computed a vertical grey level density profile along the depth of the cortical region. Second, we divided each profile into 20 bins and averaged density values across images for each bin.

#### Statistical analyses

We employed one-way ANOVA for overall comparison of markers across areas and laminar groups. For analyses that showed significant differences ( $P < 0.05$ ), we performed *post hoc* pair comparisons (Bonferroni method). We report *P*-values, *F*-statistics and degrees of freedom (shown as subscripts:  $F_{\text{between groups, within groups}}$ ). Data were tabulated in Excel (Office 365; Microsoft), and analyses were performed using MATLAB.

To demonstrate global similarities/differences among prefrontal areas using all markers simultaneously (10 parameters), we performed nonmetric multidimensional scaling (NMDS), which allows visualization of high-dimensional data into a low two-dimensional space that approximates pairwise distances between data points. Each area was initially represented using a feature vector with ten dimensions: PV+ neuron density (i) across all layers, (ii) layers II–III, (iii) layers IV–VI in areas 25 and 32 or layers V–VI in eulaminar areas 10m and 46d; PV+ to neuron ratio (iv) across all layers, (v) layers II–III, and (vi) layers IV–VI in areas 25 and 32 or layers V–VI in eulaminar areas 10m and 46d; and mean grey level values (vii) of WFA, (viii) myelin, (ix)  $\alpha\text{CaMKII}$ , and (x) GFAP. Data were *z*-scored to remove scale-related effects. We employed the NMDS algorithm of MATLAB using the stress criterion for goodness of fit. The resulting NMDS diagram displayed areas in a two-dimensional space that closely fit the Euclidean distances among areas in the high-dimensional space, in which the relative proximity of areas represents their relative similarity/dissimilarity.

#### Photography for figures

We photographed representative columns with labelling under bright field (Nissl, PV, myelin, WFA and  $\alpha\text{CaMKII}$ ) or dark field (GFAP) to assemble in figures using ADOBE ILLUSTRATOR CC software (Adobe Systems Incorporated, San José, CA, USA). We made minor adjustment of overall brightness and contrast, but did not retouch images.

## Results

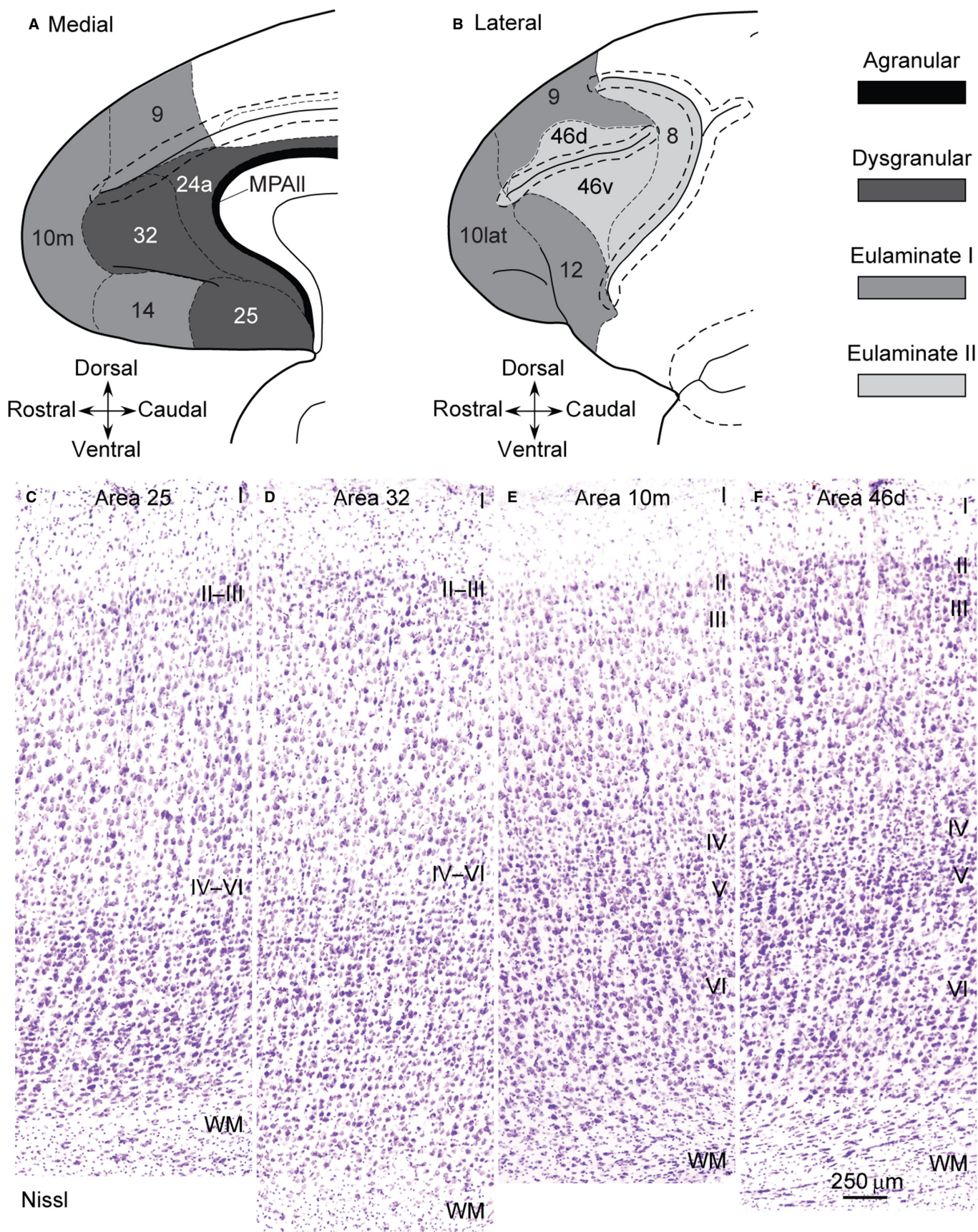
#### Progressive laminar elaboration from medial to dorsolateral prefrontal areas

Figure 1 shows the cytoarchitecture of prefrontal areas with the lowest (anterior cingulate limbic areas 25 and 32), intermediate (medial area 10, 10m) and most elaborate (dorsolateral area 46, 46d) laminar structure. These areas were used for comparison of plasticity–stability-related markers. Areas 25 and 32 are dysgranular, with a rudimentary layer IV (Fig. 1C and D). Area 10m, situated anterior to area 32, has six layers (eulaminar) and has been categorized as eulaminar I (Fig. 1E; Dombrowski *et al.*, 2001). Area 46d has the best developed lamination with a prominent layer IV and has been categorized with eulaminar II areas (Fig. 1F). There is a notable increase in neuron density in the upper layers shown in Fig. 1C–F.

#### Density of PV+ inhibitory neurons is higher in eulaminar areas

PV+ neurons were sparsely distributed in layers II–VI of area 25 and formed a thin but conspicuous band in layer V (Fig. 2A). In area 32, PV+ neurons were comparable to area 25, but were more evenly distributed in layers II–VI (Fig. 2B). Area 10m had more PV+ neurons than areas 25 or 32 (Fig. 2C), and area 46d had the most, distributed in layers II–VI (Fig. 2D).







One-way ANOVA followed by *post hoc* comparisons revealed significantly higher density of PV+ neurons (neurons/mm<sup>3</sup>) in areas 10m and 46d than in limbic areas 25 and 32 across layers (area 25 = 3736 ± 470; area 32 = 3522 ± 382; area 10m = 7167 ± 762; area 46d = 7613 ± 308; ANOVA,  $P = 0.002$ ,  $F_{3,8} = 12.19$ ; Fig. 2E). These differences were also significant for the superficial layers II–III (area 25 = 4388 ± 564; area 32 = 4638 ± 645; area 10m = 8522 ± 709; area 46d = 9797 ± 346; ANOVA,  $P = 0.001$ ,  $F_{3,8} = 14.71$ ; Fig. 2F), but not for the deep layers (IV–VI in limbic areas 25 and 32, V–VI in eulaminar areas 10m and 46d; area 25 = 4597 ± 666; area 32 = 3561 ± 503; area 10m = 6383 ± 1272; area 46d = 6255 ± 752; ANOVA,  $P = 0.24$ ,  $F_{3,8} = 1.72$ ; Fig. 2G). In layer IV of areas 10m and 46d, PV+ neuron density was higher than in other layers (area 10m = 15 906 ± 1229; area 46d = 15 877 ± 1243; Fig. 2H).

We then estimated neuron density in Nissl-stained sections as a first step to compute PV+ neurons as a proportion of the entire neuron population for each area and laminar group. Neuron density (neurons/mm<sup>3</sup>) was overall higher in eulaminar areas 10m and 46d than in limbic areas 25 and 32 across layers I–VI (area 25 = 48 652 ± 4063; area 32 = 46 695 ± 534; area 10m = 56 452 ± 5692; area 46d = 53 121 ± 3828), as well as in layers II–III (area 25 = 47 577 ± 3059; area 32 = 49 961 ± 857; area 10m = 58 954 ± 7977; area 46d = 60 463 ± 6262), but these differences were not statistically significant (ANOVA,  $P = 0.52$ ,  $F_{3,8} = 0.81$ ;  $P = 0.45$ ,  $F_{3,8} = 0.97$ ; and  $P = 0.13$ ,  $F_{3,8} = 2.53$ , respectively). The most striking difference was in layer IV of eulaminar areas 10m and 46d, which was denser than other layers (area 10m = 98 303 ± 6991; area 46d = 111 400 ± 2132) consistent with previous findings (Dombrowski *et al.*, 2001).

We then computed the density of PV+ neurons as a proportion of the entire neuron population and found that it was higher in eulaminar areas 10m and 46d than in limbic areas 25 and 32 across layers (area 25 = 0.08 ± 0.01; area 32 = 0.09 ± 0.03; area 10m = 0.13 ± 0.002; area 46d = 0.15 ± 0.02; ANOVA,  $P = 0.003$ ,  $F_{3,8} = 11.17$ ; Fig. 2I). The highest proportion of PV+ neurons was also seen in the group of superficial layers II–III (area 25 = 0.09 ± 0.01; area 32 = 0.09 ± 0.02; area 10m = 0.15 ± 0.01; area 46d = 0.17 ± 0.03; ANOVA,  $P = 0.014$ ,  $F_{3,8} = 6.81$ ; Fig. 2J), and the deep layers (layers IV–VI in limbic areas 25 and 32 or layers V–VI in eulaminar areas 10m and 46d; area 25 = 0.07 ± 0.01; area 32 = 0.07 ± 0.02; area 10m = 0.09 ± 0.01; area 46d = 0.13 ± 0.02; ANOVA,  $P = 0.011$ ,  $F_{3,8} = 7.4$ ; Fig. 2K). *Post hoc* comparisons revealed significant differences between each limbic area and eulaminar area 46d across layers, as well as for superficial layers II–III and deep layers. In layer IV of areas 10m and 46d, the proportion of PV+ neurons was comparable to layers II–III (area 10m = 0.15 ± 0.01; area 46d = 0.14 ± 0.01; Fig. 2L).

#### PNN density is higher in eulaminar areas

In area 25, there was scant PNN labelling with WFA in layers II–III, but there was a band of stronger staining in the neuropil in layer V (Fig. 3A). Area 32 had slightly more label of PNNs in layers II–III than area 25 (Fig. 3B). In area 10m, WFA staining was comparable to area 32 (Fig. 3C). In area 46d, there was more labelling of PNNs across layers II–VI than in the other areas (Fig. 3D). Layer I did not show WFA staining in any area. There was evidence of PNN label around some pyramidal neurons across areas as well (Fig. 3A, black arrow).

The above findings were corroborated by measuring the mean grey level index of WFA staining through the depth of the cortex (Fig. 3E). The variation in grey level density of WFA along the

depth of normalized columns showed an increase towards the middle layers in the four areas (Fig. 3F). The middle bins showed higher content of WFA in area 46d than in the other areas, as shown by separation of the function for this area (Fig. 3F).

#### Intracortical myelin content is higher in eulaminar areas

Area 25 had the sparsest myelinated axons, arranged in vertical arrays in layers IV–VI (Fig. 4A), a pattern that was more elaborate in area 32 (Fig. 4B). In eulaminar area 10m, vertical arrays of myelinated axons were thicker and interwoven with abundant horizontal myelinated axons in layers IV, V and VI, and there were more myelinated axons in superficial layers II–III compared with areas 25 and 32 (Fig. 4C). Eulaminar area 46d had vertical myelinated axons forming thick bundles that extended from the white matter to layer III and above, which were denser than in the other areas (Fig. 4D).

Measurement of the mean grey level index of myelin through the depth of the cortex corroborated the qualitative patterns described above (Fig. 4E). The variation in grey level density of myelin along the depth of normalized columns showed an increase towards the white matter in the four areas. The middle–deep bins showed higher content of myelin in areas 46d and 10m than in areas 25 and 32, revealed by the separation of the four functions (Fig. 4F).

#### $\alpha$ CaMKII expression is higher in limbic areas

The density of  $\alpha$ CaMKII showed the opposite trend in the four areas than PV+ neurons or myelin. In areas 25 and 32,  $\alpha$ CaMKII expression was dense in the neuropil of layers I and II and superficial part of layer III and was moderate in the deep part of layer III and layers IV–VI (brown label; Fig. 5A and B). In area 10m, expression of  $\alpha$ CaMKII was dense in layers I and II; moderate in layers III, V and VI; and light in layer IV (Fig. 5C). In area 46d,  $\alpha$ CaMKII expression was dense in layer I; moderate in layer II, superficial layer III and layer VI; and very light in the deep part of layer III, layer IV and upper layer V (Fig. 5D).

One-way ANOVA followed by *post hoc* comparisons revealed significantly lower mean grey level index of  $\alpha$ CaMKII in area 46d than in areas 25 and 32 (ANOVA,  $P = 0.001$ ,  $F_{3,4} = 57.71$ ; Fig. 5E). The variation in grey level density along the depth of normalized columns showed that  $\alpha$ CaMKII expression decreased towards the white matter in the four areas (Fig. 5F).

#### GFAP expression is higher in limbic areas, but astrocyte density is comparable across areas

Expression of GFAP, a marker of activated astrocytes, revealed a distinct and pronounced trend across the four areas. Area 25 showed dense and uniform expression of GFAP across layers (Fig. 6A, yellow label). A similar pattern was evident in area 32, with the exception of moderate expression in the middle cortical layers (Fig. 6B). In eulaminar areas 10m and 46d, dense GFAP expression was restricted to layers I and VI with moderate expression in layer II and superficial layer III, due to GFAP labelling of the processes of interlaminar astrocytes located in layer I. The deep part of layer III, layer IV and layer V had light expression of GFAP (dark region in Fig. 6C and D).

One-way ANOVA followed by *post hoc* analysis of the mean grey level index showed that areas 25 and 32 had significantly higher GFAP expression than eulaminar area 46d (ANOVA,  $P = 0.002$ ,  $F_{3,4} = 16.56$ ; Fig. 6E). The variation in grey level density along the depth of normalized columns showed that GFAP expression was higher in layer I and layer VI, while the middle part of the cortex around layer IV had the lowest level (Fig. 6F).

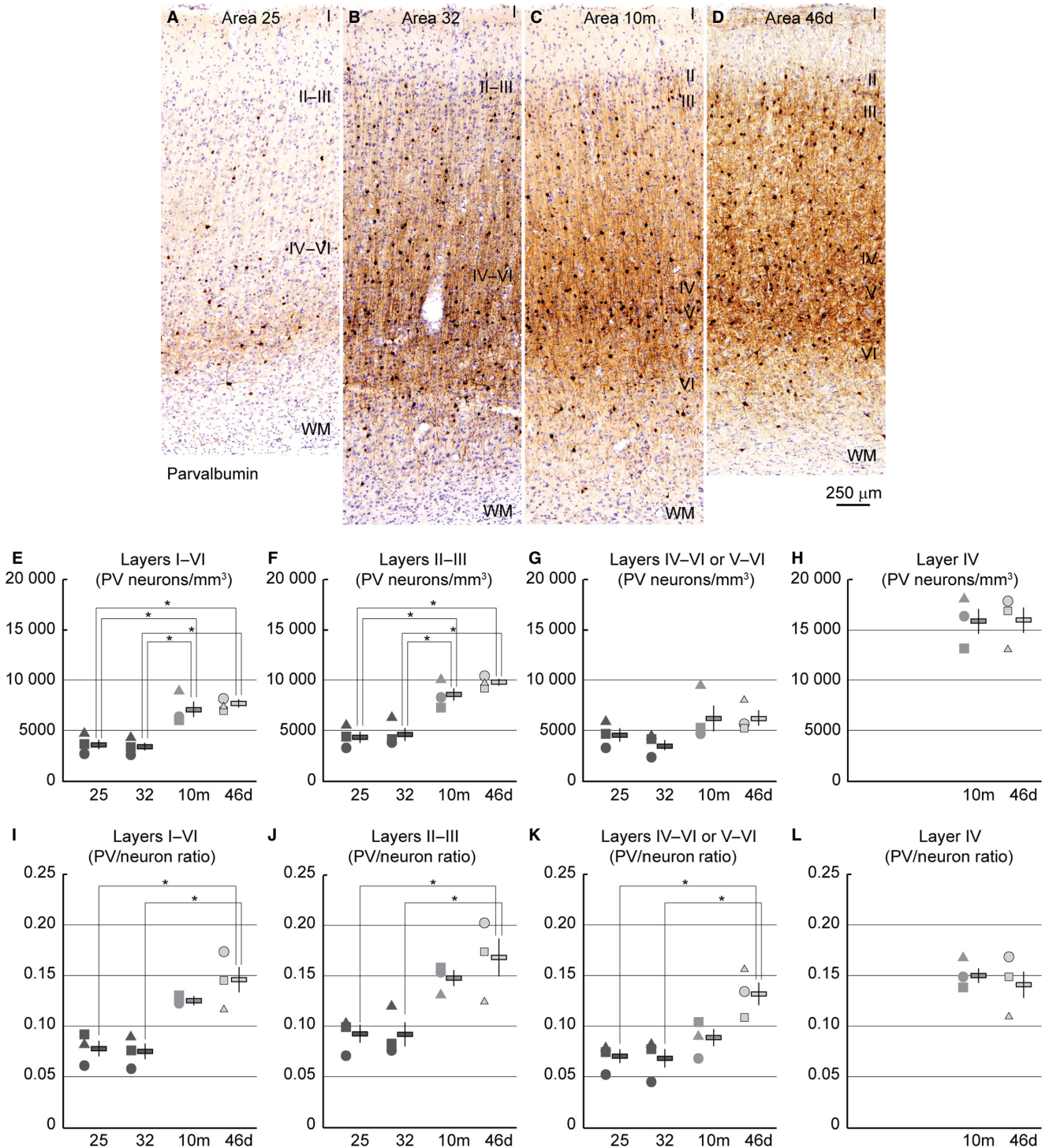


FIG. 2. Distribution of parvalbumin-positive (PV+) neurons in limbic and eulaminar areas of the monkey prefrontal cortex. (A–D) Photomicrographs of areas 25, 32, 10m and 46d. A, In area 25, PV+ neurons are sparse across layers and form a thin band in layer V. (B) PV+ neurons are more evenly distributed within layers in area 32 than in area 25. (C, D) Eulaminar areas 10m and 46d have more PV+ neurons than areas 25 and 32 with a dense band in layers IV and V. (E) PV+ neuron density is higher in eulaminar areas 10m and 46 than in areas 25 and 32 across layers. (F) PV+ neuron density is higher in eulaminar areas 10m and 46 than in areas 25 and 32 in the superficial layers. (G) PV+ neuron density is higher in eulaminar areas 10m and 46 than in areas 25 and 32 in the deep layers (IV–VI for limbic, V–VI for eulaminar). (H) Layer IV, which is distinct in areas 10m and 46d, has the highest PV+ neuron density. (I) The proportion of PV+ neurons for the entire neuron population is higher in eulaminar areas 10m and 46d than in limbic areas 25 and 32 across layers. (J) The proportion of PV+ neurons for the neuron population in superficial layers is higher in eulaminar areas 10m and 46d than in limbic areas 25 and 32. (K) The proportion of PV+ neurons for the neuron population in the deep layers is higher in eulaminar areas 10m and 46d than in limbic areas 25 and 32 (layers IV–VI for limbic, V–VI for eulaminar). (L) The proportion of PV+ neurons for the neuron population in layer IV is high in areas 10m and 46d. WM, white matter. Roman numerals indicate cortical layers. Asterisks in (E, F) and (I–K) indicate significant differences between pairs of areas, as determined by *post hoc* analysis (Bonferroni method) conducted after one-way ANOVA. Scatter plots in (E–L) represent individual cases denoted by different symbols; greyscale horizontal bars represent case averages; vertical lines on bars show the standard error. Calibration bar in D applies to A–D.



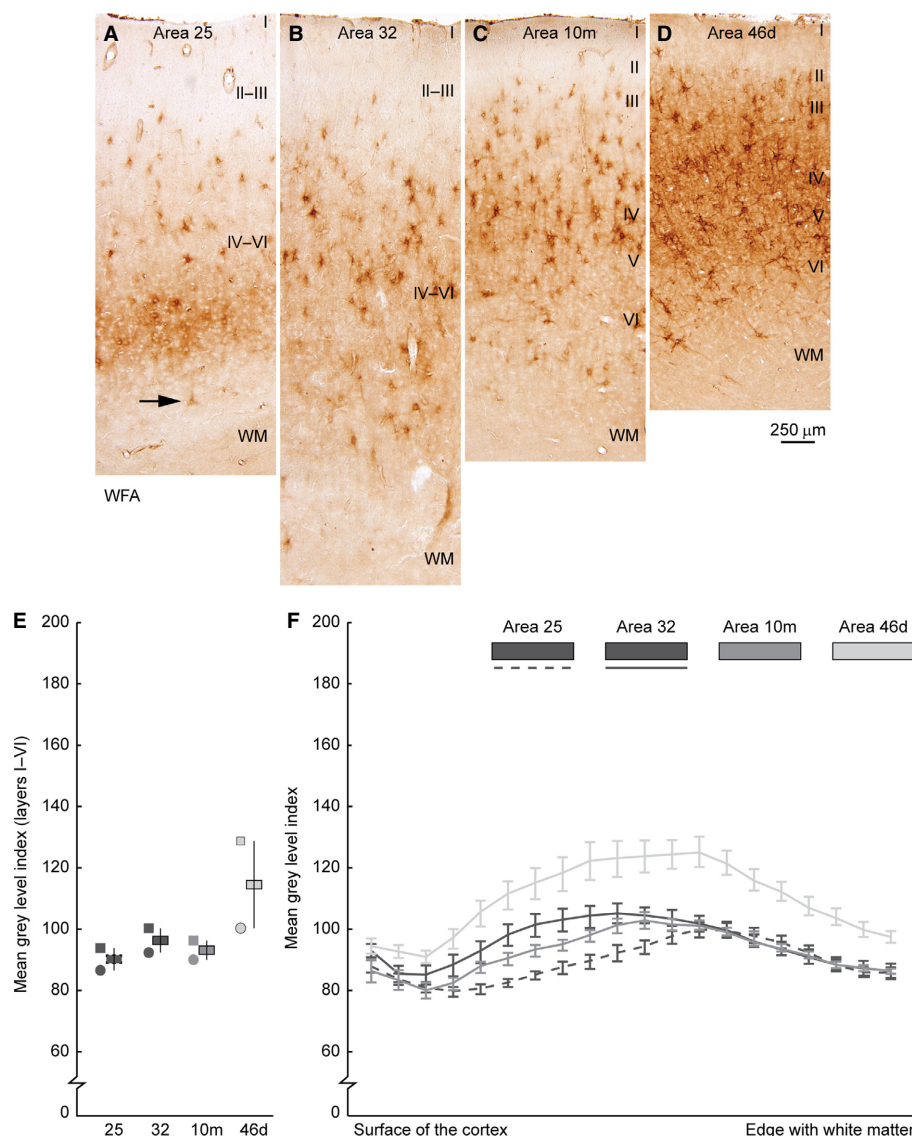


FIG. 3. Perineuronal net (PNN) label by the lectin *Wisteria floribunda* agglutinin (WFA) in limbic and eulaminar areas of the monkey prefrontal cortex. (A–D) Photomicrographs of areas 25, 32, 10m and 46d stained for WFA. (A) Area 25 shows scant label in layers II–III and a band of WFA staining in the neuropil of layer V; black arrow points at PNN in a pyramidal neuron. (B, C) Areas 32 and 10m show more label for WFA in layers II–III and IV–V than area 25. (D) Area 46d shows the highest label for WFA across layers II–VI compared to other areas. (E) The mean grey level index through the depth of the cortex shows higher levels of WFA staining in area 46d. (F) WFA content increases towards the middle layers in the four areas, shown along the course from the surface of the cortex (left) to the edge of the white matter (right); the highest density is found consistently in area 46d and the lowest in area 25. WM, white matter. Roman numerals indicate cortical layers. Scatter plots in E represent individual cases denoted by different symbols; greyscale horizontal bars represent case averages; vertical lines on bars show the standard error. Calibration bar in D applies to A–D. [Colour figure can be viewed at [wileyonlinelibrary.com](http://wileyonlinelibrary.com)].

We then estimated astrocyte density in Nissl-stained sections to investigate whether it correlated with GFAP expression or not. This analysis revealed that the densities of astrocytes in layers I–VI were not significantly different among areas (area 25 =  $22\,448 \pm 2058$ ; area 32 =  $23\,357 \pm 968$ ; area 10m =  $23\,515 \pm 1688$ ; area 46d =  $21\,515 \pm 1484$ ; ANOVA,  $P = 0.89$ ,  $F_{3,8} = 0.22$ ).

#### *Iba1* expression and microglia density are comparable across areas

Expression of the calcium binding protein Iba1, which labels resting microglia (Hendrickx *et al.*, 2017), was comparable across the areas studied. Labelled macrophages were homogeneously distributed across areas and layers forming a network that looked like a starry sky. Iba1-labelled cells had a small cell body and ramified

cytoplasm, consistent with resting microglia (Torres-Platas *et al.*, 2014). We also estimated microglia density in Nissl-stained sections and found comparable numbers across areas in layers I–VI (area 25 =  $5908 \pm 318$ ; area 32 =  $6426 \pm 495$ ; area 10m =  $6099 \pm 194$ ; area 46d =  $5688 \pm 706$ ; ANOVA,  $P = 0.83$ ,  $F_{3,8} = 0.3$ ) consistent with the above findings.

#### Overall segregation of prefrontal areas by plasticity–stability markers

Nonmetric multidimensional scaling (NMDS) made it possible to condense features along a 10-dimensional space into a two-dimensional space, to facilitate visualization while preserving differences among the four areas. NMDS revealed a clear separation between limbic (left) and eulaminar areas (right) and also showed separation

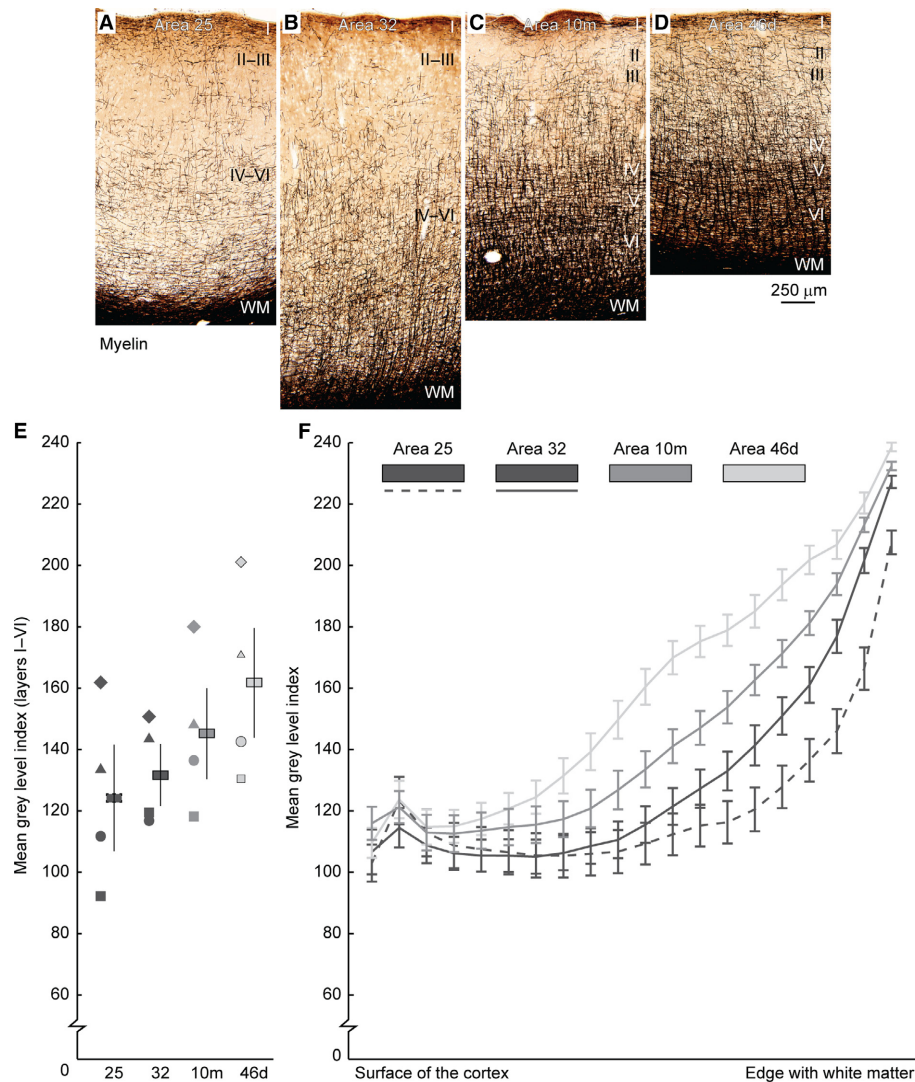


FIG. 4. Myelin content in limbic and eulaminar areas of the monkey prefrontal cortex. (A–D), Photomicrographs of areas 25, 32, 10m and 46d stained with the Gallyas technique for myelin. (A, B) In areas 25 and 32, the content of intracortical myelin is lower than in eulaminar areas. (C, D) Area 10m and area 46d show progressive increase of intracortical myelin. (E) The mean grey level index of myelin through the depth of the cortex also shows this trend. (F) Myelin content increases towards the white matter in the four areas and is higher in the middle–deep bins of areas 46d and 10m than in areas 25 and 32. WM, white matter. Roman numerals indicate cortical layers. Scatter plots in E represent individual cases denoted by different symbols; greyscale horizontal bars represent case averages; vertical lines on bars show the standard error. Calibration bar in D applies to A–D. [Colour figure can be viewed at [wileyonlinelibrary.com](http://wileyonlinelibrary.com)].

between each pair of cortices (Fig. 7). Stress was negligible ( $\sim 6 \times 10^{-17}$ ) indicating that the two-dimensional space accurately reproduced the differences among areas.

## Discussion

Our findings revealed that limbic prefrontal areas showed significantly lower expression of markers associated with stability and higher expression of the marker  $\alpha$ CaMKII associated with plasticity and GFAP, which is related to cellular stress (Sofroniew & Vinters, 2010; Hol & Pekny, 2015). In contrast, eulaminar areas showed the opposite trend. These findings were predicted from the graded increase in laminar elaboration from limbic to eulaminar areas (Barbas, 2015). This evidence suggests that the potential for synaptic plasticity is higher in limbic areas than in eulaminar areas (Barbas, 1995). These features are consistent with a key role of limbic areas in emotions, learning and memory and eulaminar prefrontal areas in cognition (Fuster, 2008; Pessoa, 2008; John *et al.*, 2013;

Anderson *et al.*, 2015; Chanes & Barrett, 2016; Barbas & García-Cabezas, 2017).

## Variation of plasticity-related markers suggests higher synaptic plasticity in limbic areas

The reshaping of neural circuits by experience in adult cortex is constrained by factors that regulate synaptic plasticity, including postsynaptic receptors and synapse turnover (Holtmaat & Svoboda, 2009; Lisman *et al.*, 2012; Takesian & Hensch, 2013; Lisman, 2017). Inhibitory circuitry limits synaptic plasticity during normal periods that follow the highly plastic critical periods, as seen by blockade of glutamic acid decarboxylase or GABA<sub>A</sub> receptors (Harauzov *et al.*, 2010; Saez & Friedlander, 2016). Specifically, digestion of PNNs around PV inhibitory neurons reverses synaptic plasticity to the critical period (Pizzorusso *et al.*, 2002; Romberg *et al.*, 2013; Lensjo *et al.*, 2017). A striking finding here is the



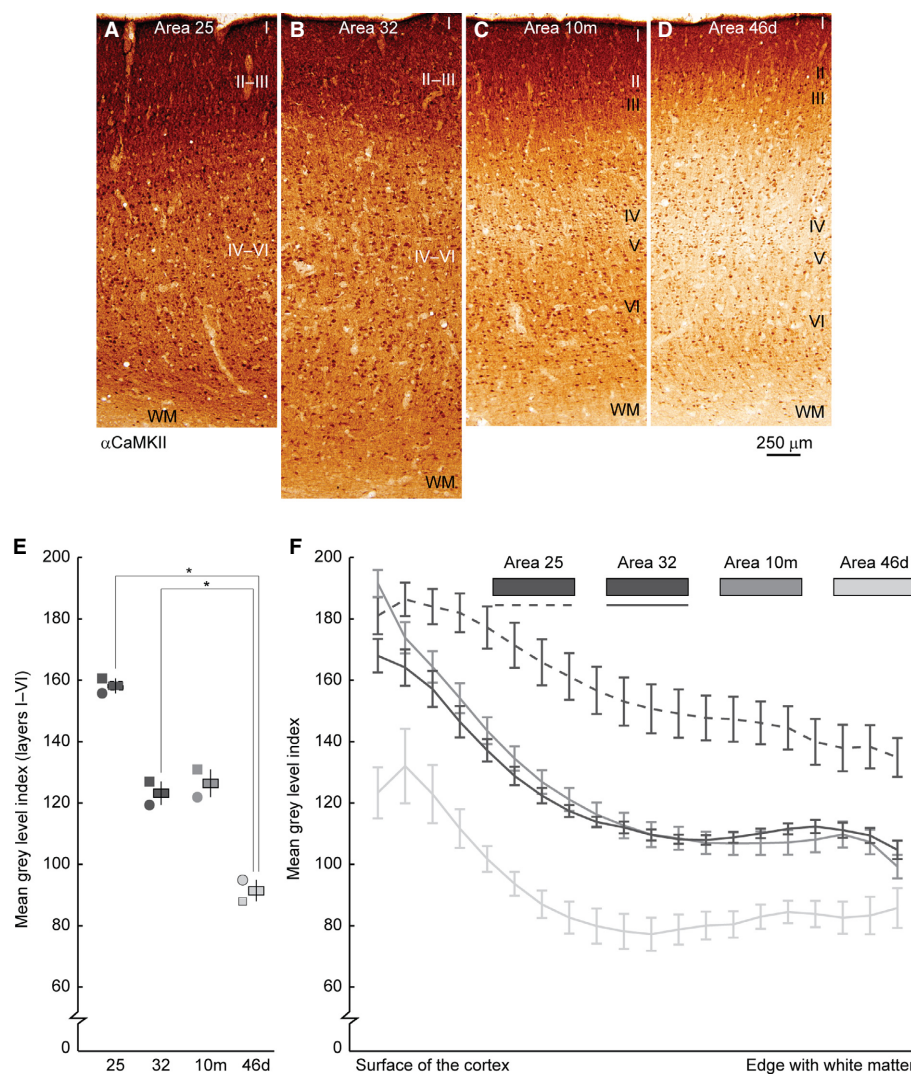


FIG. 5. Expression of the alpha subunit of the calcium/calmodulin-dependent protein kinase II ( $\alpha$ CaMKII) in limbic and eulaminar areas of the rhesus monkey prefrontal cortex. (A–D) Photomicrographs of areas 25, 32, 10m and 46d stained for  $\alpha$ CaMKII. (A) Area 25 shows high neuropil expression of  $\alpha$ CaMKII across layers (dark brown). (B, C) In area 32 and in area 10m,  $\alpha$ CaMKII expression is lower than in area 25. (D) Area 46d shows lower expression of  $\alpha$ CaMKII than areas 25, 32 and 10m across layers except in layer I. (E) The mean grey level index of  $\alpha$ CaMKII also shows the trend of (A–D). (F)  $\alpha$ CaMKII expression decreases towards the white matter in the four areas. WM, white matter. Roman numerals indicate cortical layers. Asterisks in (E) indicate significant differences between pairs of areas, as determined by *post hoc* analysis (Bonferroni method) conducted after one-way ANOVA. Scatter plots in (E) represent individual cases denoted by different symbols; greyscale horizontal bars represent case averages; vertical lines on bars show the standard error. Calibration bar in D applies to A–D.

significantly lower proportion of PV+ neurons from the entire neuron population in prefrontal limbic areas than in the best delineated eulaminar areas. The significance of this finding is based on functional evidence that PV+ neurons exert strong perisomatic inhibition of nearby pyramidal neurons (DeFelipe, 2002).

A significant proportion of PV neurons in the cerebral cortex are coated by extracellular PNNs (Hartig *et al.*, 1992, 1994). The development of PNNs coincides with the end of critical periods, and PNN removal in adult life reverts plasticity levels to critical periods (Pizzorusso *et al.*, 2002; Sorg *et al.*, 2016; Lensjo *et al.*, 2017). We found that PNN density, as labelled by WFA, is higher in eulaminar area 46d than in areas 25, 32 and 10m. Comparable patterns of labelling of WFA across prefrontal areas were found in the cebus monkey (Cruz-Rizzolo *et al.*, 2011).

The pattern of myelin content followed a similar trend as PV neuron density. Myelin-associated proteins limit cortical synaptic plasticity, spine turnover and LTP (Akbik *et al.*, 2013; Schwab & Strittmatter,

2014; Boghdadi *et al.*, 2017). This pattern is consistent with more elaborate dendritic trees and more spines in limbic than in eulaminar areas in the prefrontal cortex of primates (Elston *et al.*, 2005a,b,c, 2006, 2011; Sasaki *et al.*, 2015; Medalla *et al.*, 2017).

In contrast,  $\alpha$ CaMKII, which is a key modulator of synaptic plasticity and crucial for LTP (Lisman *et al.*, 2012), showed high expression in the neuropil of limbic area 25 and was intermediate in areas 32 and 10m and low in area 46d. In area 46d, only layer I had high expression of  $\alpha$ CaMKII. These findings may reflect differences in spine labelling and suggest that in limbic areas, LTP is facilitated across layers. In contrast, in area 46d LTP may be more easily attained in layer I, which also lacks PV neurons and PNNs and is the major recipient of feedback projections from areas with less elaborate laminar structure, including limbic areas (Barbas, 2015).

As summarized in Fig. 8, the opposite trends in the expression of plasticity and stability markers suggest that prefrontal limbic areas

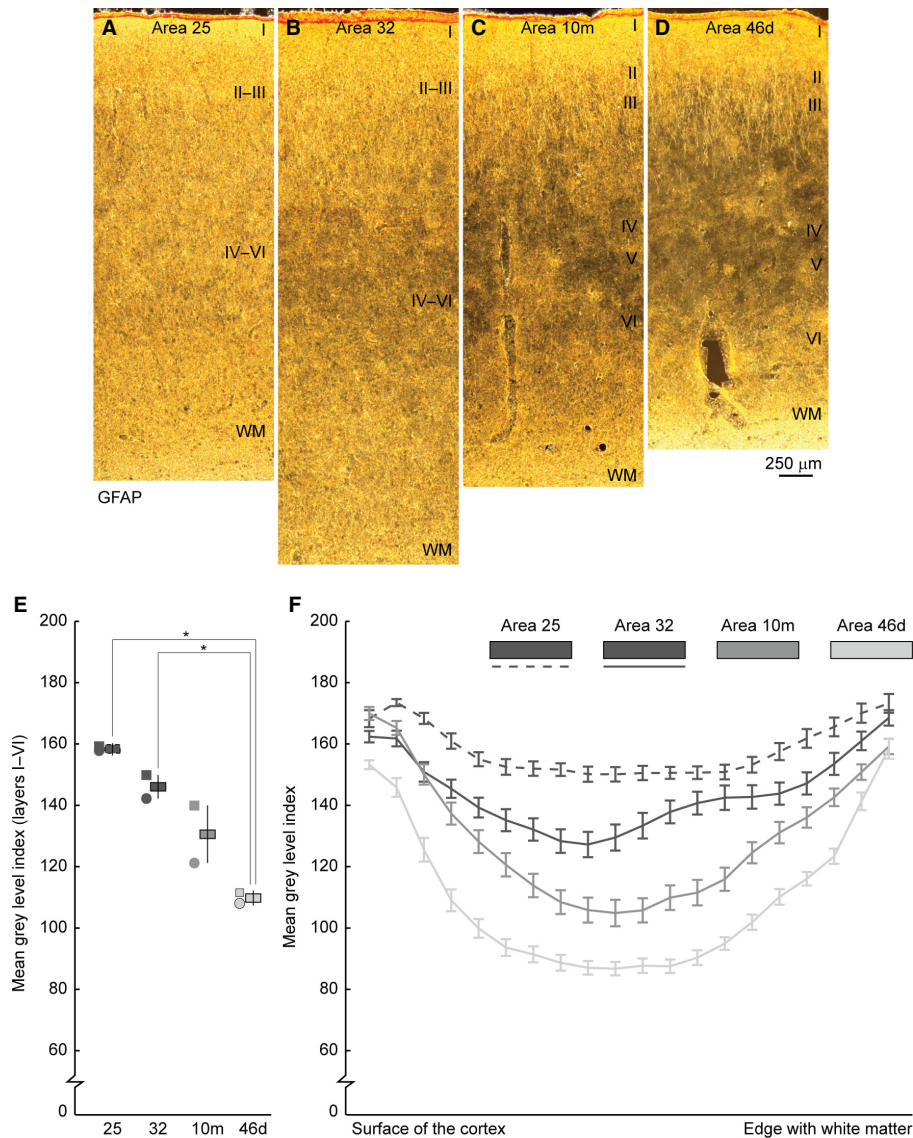


FIG. 6. Expression of glial fibrillary acidic protein (GFAP) in limbic and eulaminar prefrontal areas in rhesus monkeys. (A–D) Photomicrographs of areas 25, 32, 10m and 46d stained using immunohistochemistry for GFAP (gold label). (A) Area 25 shows dense GFAP labelling across layers. (B) GFAP labelling is also dense in area 32, but the middle layers show moderate labelling (less gold labelling). (C, D) The middle layers in eulaminar areas 10m and 46d show light labelling of GFAP with dense expression in layers I, II and VI. (E) The mean grey level index of GFAP through the depth of the cortex also shows this trend. (F) GFAP expression decreases from layer I and the white matter towards the middle part of the cortex in the four areas, a pattern that is more pronounced in eulaminar areas 10m and 46d. WM, white matter. Roman numerals indicate cortical layers. Asterisks in (E) indicate significant differences between pairs of areas, as determined by *post hoc* analysis (Bonferroni method) conducted after one-way ANOVA. Scatter plots in (E) represent individual cases denoted by different symbols; greyscale horizontal bars represent case averages; vertical lines on bars show the standard error. Calibration bar in D applies to A–D.

are more plastic than eulaminar areas. In contrast, eulaminar cortices with the best delineated laminar structure may be more stable.

#### GFAP expression suggests more activation of astrocytes in limbic areas

We found comparable densities of astrocytes and microglia across limbic and eulaminar areas. The distribution of cells labelled for Iba1, a marker that labels resting microglia, was also comparable across areas. Iba1-labelled cells across areas in our material showed features of resting microglia and comparable levels across areas. In contrast, labelling for GFAP, a marker of activated astrocytes (Sofroniew & Vinters, 2010; Hol & Pekny, 2015), was higher in limbic areas 25 and 32 than in eulaminar area 10m and especially

in area 46d, which has the best delineated laminar structure. This evidence suggests that astrocytes in limbic cortices normally have higher levels of cellular stress. Astrocytes can impact synaptic plasticity because they participate in cellular and molecular processes related to synapse and neurotransmitter regulation (Singh & Abraham, 2017). The higher expression of GFAP in limbic areas may reflect higher demands of neurons engaged in synaptic plasticity functions.

#### Plasticity–stability trends along the cerebral cortex

Our analysis focused on four representative prefrontal areas, but data in the literature suggest comparable distribution of markers associated with plasticity and stability across the primate cerebral cortex.



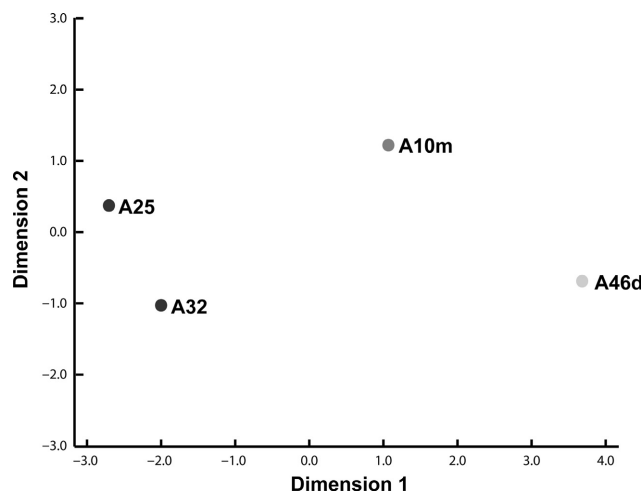


FIG. 7. Nonmetric multidimensional scaling (NMDS) diagram shows separation between limbic areas 25 and 32 (left) and eulamine areas 10m and 46d (right) with a negligible level of stress ( $\sim 6 \times 10^{-17}$ ), indicating that the two-dimensional space accurately reproduced the differences among areas.

For instance, PV expression and PNN density vary in the human temporal areas (Ding *et al.*, 2009) with a notable increase progressively from limbic to eulamine areas. Similarly, classical studies

have shown that intracortical myelin increases from limbic to eulamine areas in all lobes and systems of the primate brain (Sanides, 1970). At the other extreme of the plasticity–stability spectrum, expression in adult cortex of the growth-associated phosphoprotein 43 (GAP-43), a marker related to synaptic plasticity and LTP (Benowitz *et al.*, 1989; Benowitz & Routtenberg, 1997), has a complementary expression to myelin, with much higher expression in limbic areas than in eulamine cortices; the latter include the highly differentiated primary areas (Benowitz *et al.*, 1989). Other cellular features also vary in parallel with laminar elaboration in the cortex and the expression of plasticity–stability-related markers. For instance, in the monkey temporal and frontal lobes spine density and the length of dendritic arborization vary consistently across cortical areas (Elston, 2003; Elston *et al.*, 2005a,b,c, 2006; Sasaki *et al.*, 2015; Medalla *et al.*, 2017). Laminar elaboration in inferior temporal and occipital areas of the macaque monkey increases in the anterior-to-posterior direction as shown in fig. 9 of Hilgetag *et al.* (2016). In the same areas, spine density, dendritic size and dendritic complexity decrease in the anterior-to-posterior direction as shown in fig. 6 of Elston (2003). These structural features show steady changes across areas in parallel with changes in elaboration of laminar structure from limbic to eulamine cortices.

Our findings, along with observations from the literature, suggest that limbic areas, which are found at the foot of every cortical

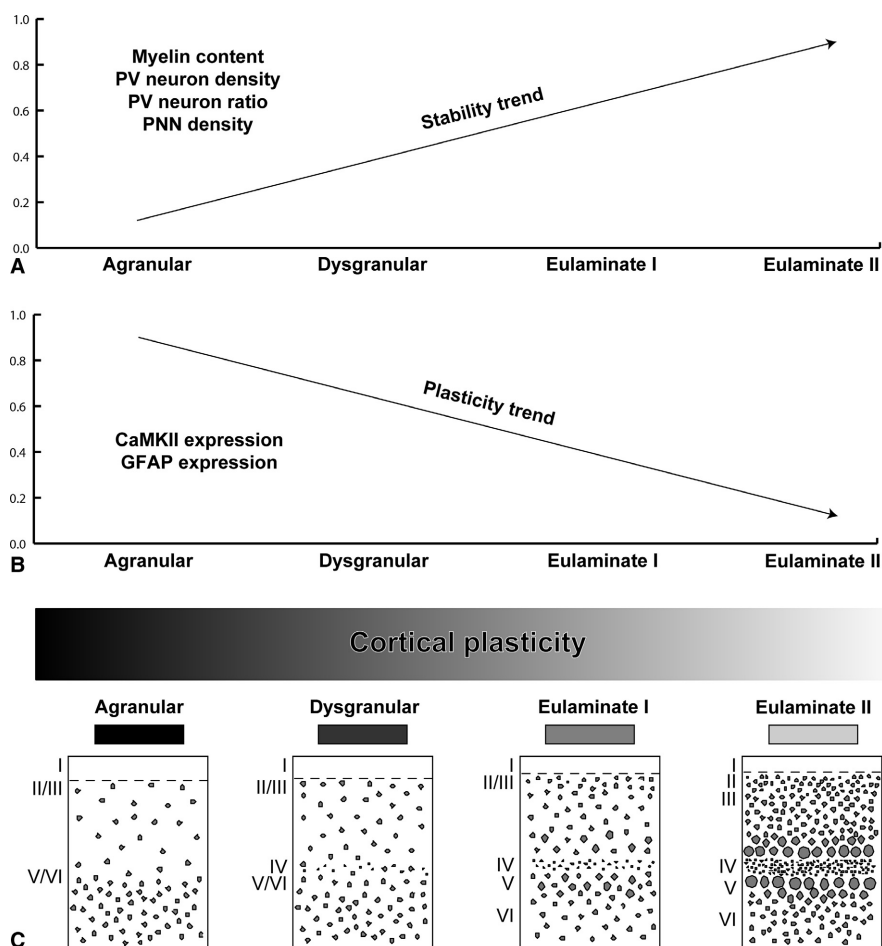


FIG. 8. Markers of plasticity in the cortex parallel laminar differentiation. (A) Cartoon depicts expression of factors that limit synaptic plasticity, which are higher in eulamine than in limbic areas. (B) Conversely, expression of  $\alpha$ CaMKII, known to enhance synaptic plasticity, is higher in limbic areas; GFAP expression, a marker of cellular stress, is also higher in limbic areas than in eulamine areas. (C) The distribution of these markers suggests that cortical plasticity and stability change systematically with laminar differentiation as shown in the cartoon of cellular density across areas.

system (Barbas, 1986, 1988), are more plastic, and their neurons have larger dendritic arbours with more spines, consistent with their multimodal, associative functions. In contrast, eulaminate areas across systems are more stable along the axis of increasing laminar elaboration. Pyramidal neurons in eulaminate areas have smaller dendritic trees with fewer spines, consistent with more specialized functions, a pattern accentuated in the highly laminated primary sensory cortices (Barbas, 2015).

### Plasticity–stability features and implications for pathology

Cortical areas are not equally susceptible to neurologic and psychiatric diseases. For example, aggregation of tau protein in Alzheimer's and  $\alpha$ -synuclein in Parkinson's disease starts in limbic cortices and spreads gradually towards eulaminate areas (Arnold *et al.*, 1991; Duyckaerts *et al.*, 1998; Braak *et al.*, 2006; Brettschneider *et al.*, 2015). Similarly, the lower density of the powerful PV neurons may render limbic cortices vulnerable to epileptiform activity (Barbas, 1995; Zikopoulos & Barbas, 2013). Anterior cingulate limbic areas, including areas 25 and 32, are also preferentially implicated in psychiatric diseases such as depression (Mayberg *et al.*, 2005) and autism (Zikopoulos & Barbas, 2010, 2013).

The observation of differential involvement of areas in neurologic and psychiatric diseases led Oskar and Cécile Vogt to propose the idea of pathocllisis, or selective vulnerability. The Vogts speculated that specific differences in the physicochemical composition of cells provided the basis for differences in susceptibility to insult and disease in different brain regions, although there was little evidence to substantiate the idea at the cellular and molecular levels (Vogt & Vogt, 1922; Klatzo, 2003). Based on novel findings here, we suggest that the complement of cellular and molecular features at once endows limbic areas with plasticity but also vulnerability to disruption in disease. High plasticity entails high metabolic activity and cellular stress, as revealed by higher expression of GFAP in anterior cingulate limbic areas compared with eulaminate cortices. These findings provide the basis to investigate in future studies factors that facilitate the highly plastic processes of learning, emotions and memory, as well as the trigger that leads to disruption and pathology in neurologic and psychiatric diseases.

### Acknowledgements

This work was supported by the National Institutes of Health (National Institute of Neurological Disorders and Stroke, grant number R01NS024760; National Institute of Mental Health, grant numbers R01MH057414 and R01MH101209); and by the Center of Excellence for Learning in Education, Science and Technology (CELEST), a National Science Foundation Science of Learning Center (grant number NSF SBE-0354378). M. Á. García-Cabezas was the recipient of a 2014 NARSAD Young Investigator Grant from the Brain and Behavior Research Foundation (grant number 22777, P&S Fund Investigator).

### Conflict of interest

Nothing to declare.

### Author contributions

MAG-C designed the experiments, conducted analyses, prepared figures and wrote the manuscript. MKJ performed stereological counts and analysis of PV neuron densities. YJJ performed image processing and statistical analyses. BZ designed analysis and provided input for the manuscript. HB designed the experiments and analyses and

wrote the manuscript. All the authors read and approved the manuscript.

### Data accessibility

Supporting data will be made available upon request to the corresponding author.

### Abbreviations

$\alpha$ CaMKII, alpha subunit of calcium/calmodulin-dependent protein kinase II; GFAP, glial fibrillary acidic protein; Iba1, ionized calcium binding adapter molecule 1; LTD, long-term depression; LTP, long-term potentiation; NMDS, nonmetric multidimensional scaling; PNNs, perineuronal nets; PV, parvalbumin; WFA, lectin *Wisteria floribunda* agglutinin; WM, white matter.

### References

- Akbik, F., Cafferty, W.B. & Strittmatter, S.M. (2012) Myelin associated inhibitors: a link between injury-induced and experience-dependent plasticity. *Exp. Neurol.*, **235**, 43–52.
- Akbik, F.V., Bhagat, S.M., Patel, P.R., Cafferty, W.B. & Strittmatter, S.M. (2013) Anatomical plasticity of adult brain is titrated by Nogo Receptor 1. *Neuron*, **77**, 859–866.
- Anderson, M.C., Bunce, J.G. & Barbas, H. (2015) Prefrontal-hippocampal pathways underlying inhibitory control over memory. *Neurobiol. Learn. Mem.*, **134**(Pt A), 145–161.
- Arnold, S.E., Hyman, B.T., Flory, J., Damasio, A.R. & Van Hoesen, G.W. (1991) The topographical and neuroanatomical distribution of neurofibrillary tangles and neuritic plaques in the cerebral cortex of patients with Alzheimer's disease. *Cereb. Cortex*, **1**, 103–116.
- Barbas, H. (1986) Pattern in the laminar origin of corticocortical connections. *J. Comp. Neurol.*, **252**, 415–422.
- Barbas, H. (1988) Anatomic organization of basoventral and mediadorsal visual recipient prefrontal regions in the rhesus monkey. *J. Comp. Neurol.*, **276**, 313–342.
- Barbas, H. (1993) Organization of cortical afferent input to orbitofrontal areas in the rhesus monkey. *Neuroscience*, **56**, 841–864.
- Barbas, H. (1995) Anatomic basis of cognitive-emotional interactions in the primate prefrontal cortex. *Neurosci. Biobehav. R.*, **19**, 499–510.
- Barbas, H. (2015) General cortical and special prefrontal connections: principles from structure to function. *Annu. Rev. Neurosci.*, **38**, 269–289.
- Barbas, H. & García-Cabezas, M.A. (2015) Motor cortex layer 4: less is more. *Trends Neurosci.*, **38**, 259–261.
- Barbas, H. & García-Cabezas, M.A. (2017). Prefrontal cortex integration of emotions and cognition. In Watanabe, M. (Ed.), *Prefrontal Cortex as an Executive, Emotional and Social Brain*. Springer, Japan, pp. 51–76.
- Barbas, H. & Pandya, D.N. (1987) Architecture and frontal cortical connections of the premotor cortex (area 6) in the rhesus monkey. *J. Comp. Neurol.*, **256**, 211–218.
- Barbas, H. & Pandya, D.N. (1989) Architecture and intrinsic connections of the prefrontal cortex in the rhesus monkey. *J. Comp. Neurol.*, **286**, 353–375.
- Benowitz, L.I. & Routtenberg, A. (1997) GAP-43: an intrinsic determinant of neuronal development and plasticity. *Trends Neurosci.*, **20**, 84–91.
- Benowitz, L.I., Perrone-Bizzozero, N.I., Finklestein, S.P. & Bird, E.D. (1989) Localization of the growth-associated phosphoprotein GAP-43 (B-50, F1) in the human cerebral cortex. *J. Neurosci.*, **9**, 990–995.
- Berlucchi, G. & Buchtel, H.A. (2009) Neuronal plasticity: historical roots and evolution of meaning. *Exp. Brain Res.*, **192**, 307–319.
- Boghdadi, A.G., Teo, L. & Bourne, J.A. (2017) The involvement of the Myelin-associated inhibitors and their receptors in CNS plasticity and injury. *Mol. Neurobiol.* <https://doi.org/10.1007/s12035-12017-10433-12036>. [Epub ahead of print].
- Braak, H., Bohl, J.R., Muller, C.M., Rub, U., de Vos, R.A. & Del Tredici, K. (2006) Stanley Fahn Lecture 2005: The staging procedure for the inclusion body pathology associated with sporadic Parkinson's disease reconsidered. *Movement Disord.*, **21**, 2042–2051.
- Brettschneider, J., Del Tredici, K., Lee, V.M. & Trojanowski, J.Q. (2015) Spreading of pathology in neurodegenerative diseases: a focus on human studies. *Nat. Rev. Neurosci.*, **16**, 109–120.
- Chanes, L. & Barrett, L.F. (2016) Redefining the role of limbic areas in cortical processing. *Trends Cogn. Sci.*, **20**, 96–106.



- Colgan, L.A. & Yasuda, R. (2014) Plasticity of dendritic spines: subcompartmentalization of signaling. *Annu. Rev. Physiol.*, **76**, 365–385.
- Cooke, S.F. & Bear, M.F. (2014) How the mechanisms of long-term synaptic potentiation and depression serve experience-dependent plasticity in primary visual cortex. *Philos. T. Roy. Soc. B*, **369**, 20130284.
- Crúz-Rizzolo, R.J., De Lima, M.A., Ervolino, E., de Oliveira, J.A. & Casatti, C.A. (2011) Cyto-, myelo- and chemoarchitecture of the prefrontal cortex of the Cebus monkey. *BMC Neurosci.*, **12**, 6.
- DeFelipe, J. (1997) Types of neurons, synaptic connections and chemical characteristics of cells immunoreactive for calbindin-D28K, parvalbumin and calretinin in the neocortex. *J. Chem. Neuroanat.*, **14**, 1–19.
- DeFelipe, J. (2002) Cortical interneurons: from Cajal to 2001. *Prog. Brain Res.*, **136**, 215–238.
- Ding, S.L., Van Hoesen, G.W., Cassell, M.D. & Poremba, A. (2009) Parcelation of human temporal polar cortex: a combined analysis of multiple cytoarchitectonic, chemoarchitectonic, and pathological markers. *J. Comp. Neurol.*, **514**, 595–623.
- Dombrowski, S.M. & Barbas, H. (1996) Differential expression of NADPH diaphorase in functionally distinct prefrontal cortices in the rhesus monkey. *Neuroscience*, **72**, 49–62.
- Dombrowski, S.M., Hilgetag, C.C. & Barbas, H. (2001) Quantitative architecture distinguishes prefrontal cortical systems in the rhesus monkey. *Cereb. Cortex*, **11**, 975–988.
- Duyckaerts, C., Colle, M.A., Dessi, F., Piette, F. & Hauw, J.J. (1998) Progression of Alzheimer histopathological changes. *Acta Neurol. Belg.*, **98**, 180–185.
- Elston, G.N. (2003) Cortex, cognition and the cell: new insights into the pyramidal neuron and prefrontal function. *Cereb. Cortex*, **13**, 1124–1138.
- Elston, G.N. & Fujita, I. (2014) Pyramidal cell development: postnatal spino-genesis, dendritic growth, axon growth, and electrophysiology. *Front. Neuroanat.*, **8**, 78.
- Elston, G.N., Benavides-Piccione, R. & DeFelipe, J. (2005a) A study of pyramidal cell structure in the cingulate cortex of the macaque monkey with comparative notes on inferotemporal and primary visual cortex. *Cereb. Cortex*, **15**, 64–73.
- Elston, G.N., Benavides-Piccione, R., Elston, A., DeFelipe, J. & Manger, P. (2005b) Specialization in pyramidal cell structure in the cingulate cortex of the Chacma baboon (*Papio ursinus*): an intracellular injection study of the posterior and anterior cingulate gyrus with comparative notes on the macaque and vervet monkeys. *Neurosci. Lett.*, **387**, 130–135.
- Elston, G.N., Benavides-Piccione, R., Elston, A., Manger, P. & Defelipe, J. (2005c) Regional specialization in pyramidal cell structure in the limbic cortex of the vervet monkey (*Cercopithecus pygerythrus*): an intracellular injection study of the anterior and posterior cingulate gyrus. *Exp. Brain Res.*, **167**, 315–323.
- Elston, G.N., Benavides-Piccione, R., Elston, A., Zietsch, B., Defelipe, J., Manger, P., Casagrande, V. & Kaas, J.H. (2006) Specializations of the granular prefrontal cortex of primates: implications for cognitive processing. *Anat. Rec. Part A*, **288**, 26–35.
- Elston, G.N., Benavides-Piccione, R., Elston, A., Manger, P.R. & Defelipe, J. (2011) Pyramidal cells in prefrontal cortex of primates: marked differences in neuronal structure among species. *Front. Neuroanat.*, **5**, 2.
- Fuster, J.M. (2008). *The Prefrontal Cortex*. Elsevier/Academic Press, London, UK.
- Gallyas, F. (1979) Silver staining of myelin by means of physical development. *Neurol. Res.*, **1**, 203–209.
- García-Cabezas, M.A. & Barbas, H. (2014a) Area 4 has layer IV in adult primates. *Eur. J. Neurosci.*, **39**, 1824–1834.
- García-Cabezas, M.A. & Barbas, H. (2014b) A direct anterior cingulate pathway to the primate primary olfactory cortex may control attention to olfaction. *Brain Struct. Funct.*, **219**, 1735–1754.
- García-Cabezas, M.A. & Barbas, H. (2017) Anterior cingulate pathways may affect emotions through orbitofrontal cortex. *Cereb. Cortex*, **27**, 4891–4910.
- García-Cabezas, M.A., John, Y.J., Barbas, H. & Zikopoulos, B. (2016) Distinction of neurons, glia and endothelial cells in the cerebral cortex: an algorithm based on cytological features. *Front. Neuroanat.*, **10**, 107.
- Ghashghaei, H.T., Hilgetag, C.C. & Barbas, H. (2007) Sequence of information processing for emotions based on the anatomic dialogue between prefrontal cortex and amygdala. *Neuroimage*, **34**, 905–923.
- Gogolla, N., Galimberti, I. & Caroni, P. (2007) Structural plasticity of axon terminals in the adult. *Curr. Opin. Neurobiol.*, **17**, 516–524.
- Gundersen, H.J. (1986) Stereology of arbitrary particles. A review of unbiased number and size estimators and the presentation of some new ones, in memory of William R. Thompson. *J. Microsc.*, **143**(Pt 1), 3–45.
- Harauzov, A., Spolidoro, M., DiCristo, G., De Pasquale, R., Cancedda, L., Pizzorusso, T., Viegi, A., Berardi, N. *et al.* (2010) Reducing intracortical inhibition in the adult visual cortex promotes ocular dominance plasticity. *J. Neurosci.*, **30**, 361–371.
- Hartig, W., Brauer, K. & Bruckner, G. (1992) Wisteria floribunda agglutinin-labelled nets surround parvalbumin-containing neurons. *Neuroreport*, **3**, 869–872.
- Hartig, W., Brauer, K., Bigl, V. & Bruckner, G. (1994) Chondroitin sulfate proteoglycan-immunoreactivity of lectin-labeled perineuronal nets around parvalbumin-containing neurons. *Brain Res.*, **635**, 307–311.
- Hendrickx, D.A.E., van Eden, C.G., Schuurman, K.G., Hamann, J. & Huitinga, I. (2017) Staining of HLA-DR, Iba1 and CD68 in human microglia reveals partially overlapping expression depending on cellular morphology and pathology. *J. Neuroimmunol.*, **309**, 12–22.
- Hilgetag, C.C., Medalla, M., Beul, S. & Barbas, H. (2016) The primate connectome in context: principles of connections of the cortical visual system. *Neuroimage*, **134**, 685–702.
- Hol, E.M. & Pekny, M. (2015) Glial fibrillary acidic protein (GFAP) and the astrocyte intermediate filament system in diseases of the central nervous system. *Curr. Opin. Cell Biol.*, **32**, 121–130.
- Holtmaat, A. & Svoboda, K. (2009) Experience-dependent structural synaptic plasticity in the mammalian brain. *Nat. Rev. Neurosci.*, **10**, 647–658.
- Holtmaat, A., Randall, J. & Cane, M. (2013) Optical imaging of structural and functional synaptic plasticity in vivo. *Eur. J. Pharmacol.*, **719**, 128–136.
- Howard, C.V. & Reed, M.G. (1998). *Unbiased Stereology, Three-Dimensional Measurement in Microscopy*. BIOS Scientific Publishers Limited, Oxford, UK.
- Ito, D., Imai, Y., Ohsawa, K., Nakajima, K., Fukuuchi, Y. & Kohsaka, S. (1998) Microglia-specific localisation of a novel calcium binding protein, Iba1. *Brain Res. Mol. Brain Res.*, **57**, 1–9.
- John, Y.J., Bullock, D., Zikopoulos, B. & Barbas, H. (2013) Anatomy and computational modeling of networks underlying cognitive-emotional interaction. *Front. Hum. Neurosci.*, **7**, 101.
- Klatzo, I. (2003) Cecile & Oskar Vogt: the significance of their contributions in modern neuroscience. *Acta Neurochir. Suppl.*, **86**, 29–32.
- Lensjo, K.K., Lepperød, M.E., Dick, G., Hafting, T. & Fyhn, M. (2017) Removal of perineuronal nets unlocks juvenile plasticity through network mechanisms of decreased inhibition and increased gamma activity. *J. Neurosci.*, **37**, 1269–1283.
- Lisman, J. (2017) Glutamatergic synapses are structurally and biochemically complex because of multiple plasticity processes: long-term potentiation, long-term depression, short-term potentiation and scaling. *Philos. T. Roy. Soc. B*, **372**, 20160260. <https://doi.org/10.1098/rstb.2016.0260>. [Epub ahead of print].
- Lisman, J., Yasuda, R. & Raghavachari, S. (2012) Mechanisms of CaMKII action in long-term potentiation. *Nat. Rev. Neurosci.*, **13**, 169–182.
- Mayberg, H.S., Lozano, A.M., Voon, V., McNeely, H.E., Seminowicz, D., Hamani, C., Schwab, J.M. & Kennedy, S.H. (2005) Deep brain stimulation for treatment-resistant depression. *Neuron*, **45**, 651–660.
- Medalla, M. & Luebke, J.I. (2015) Diversity of glutamatergic synaptic strength in lateral prefrontal versus primary visual cortices in the rhesus monkey. *J. Neurosci.*, **35**, 112–127.
- Medalla, M., Gilman, J.P., Wang, J.Y. & Luebke, J.I. (2017) Strength and diversity of inhibitory signaling differentiates primate anterior cingulate from lateral prefrontal cortex. *J. Neurosci.*, **37**, 4717–4734.
- Nabel, E.M. & Morishita, H. (2013) Regulating critical period plasticity: insight from the visual system to fear circuitry for therapeutic interventions. *Front. Psychiatry*, **4**, 146.
- Nieuwenhuys, R. (2013) The myeloarchitectonic studies on the human cerebral cortex of the Vogt-Vogt school, and their significance for the interpretation of functional neuroimaging data. *Brain Struct. Funct.*, **218**, 303–352.
- Paillard, J. (1976) Réflexions sur l'usage du concept de plasticité en neurobiologie. *J. Psychol.*, **1**, 33–47.
- Pessoa, L. (2008) On the relationship between emotion and cognition. *Nat. Rev. Neurosci.*, **9**, 148–158.
- Pizzorusso, T., Medini, P., Berardi, N., Chierzi, S., Fawcett, J.W. & Maffei, L. (2002) Reactivation of ocular dominance plasticity in the adult visual cortex. *Science*, **298**, 1248–1251.
- Romberg, C., Yang, S., Melani, R., Andrews, M.R., Horner, A.E., Spillanti, M.G., Bussey, T.J., Fawcett, J.W. *et al.* (2013) Depletion of perineuronal nets enhances recognition memory and long-term depression in the perirhinal cortex. *J. Neurosci.*, **33**, 7057–7065.

- Rosene, D.L., Roy, N.J. & Davis, B.J. (1986) A cryoprotection method that facilitates cutting frozen sections of whole monkey brains from histological and histochemical processing without freezing artifact. *J. Histochem. Cytochem.*, **34**, 1301–1315.
- Saez, I. & Friedlander, M.J. (2016) Role of GABAA-mediated inhibition and functional assortment of synapses onto individual layer 4 neurons in regulating plasticity expression in visual cortex. *PLoS One*, **11**, e0147642.
- Sanides, F. (1970). Functional architecture of motor and sensory cortices in primates in the light of a new concept of neocortex evolution. In Noback, C.R. & Montagna, W. (Eds), *The Primate Brain: Advances in Primatology*. Appleton-Century-Crofts Educational Division/Meredith Corporation, New York, NY, pp. 137–208.
- Sasaki, T., Aoi, H., Oga, T., Fujita, I. & Ichinohe, N. (2015) Postnatal development of dendritic structure of layer III pyramidal neurons in the medial prefrontal cortex of marmoset. *Brain Struct. Funct.*, **220**, 3245–3258.
- Schwab, M.E. & Strittmatter, S.M. (2014) Nogo limits neural plasticity and recovery from injury. *Curr. Opin. Neurobiol.*, **27**, 53–60.
- Shipton, O.A. & Paulsen, O. (2014) GluN2A and GluN2B subunit-containing NMDA receptors in hippocampal plasticity. *Philos. T. Roy. Soc. B*, **369**, 20130163.
- Singh, A. & Abraham, W.C. (2017) Astrocytes and synaptic plasticity in health and disease. *Exp. Brain Res.*, **235**, 1645–1655.
- Sofroniew, M.V. & Vinters, H.V. (2010) Astrocytes: biology and pathology. *Acta Neuropathol.*, **119**, 7–35.
- Sorg, B.A., Berretta, S., Blacktop, J.M., Fawcett, J.W., Kitagawa, H., Kwok, J.C. & Miquel, M. (2016) Casting a wide net: role of perineuronal nets in neural plasticity. *J. Neurosci.*, **36**, 11459–11468.
- Takesian, A.E. & Hensch, T.K. (2013) Balancing plasticity/stability across brain development. *Prog. Brain Res.*, **207**, 3–34.
- Torres-Platas, S.G., Comeau, S., Rachalski, A., Bo, G.D., Cruceanu, C., Turceci, G., Giros, B. & Mechawar, N. (2014) Morphometric characterization of microglial phenotypes in human cerebral cortex. *J. Neuroinflamm.*, **11**, 12.
- Vogt, C. & Vogt, O. (1922) Erkrankungen der Grosshirnrinde im Lichte der Topistik - Pathoklise und Pathoarchitektonik. *J. Psychol. Neurol.*, **28**, 1–171.
- Will, B., Dalrymple-Alford, J., Wolff, M. & Cassel, J.C. (2008) The concept of brain plasticity–Paillard's systemic analysis and emphasis on structure and function (followed by the translation of a seminal paper by Paillard on plasticity). *Behav. Brain Res.*, **192**, 2–7.
- Zikopoulos, B. & Barbas, H. (2006) Prefrontal projections to the thalamic reticular nucleus form a unique circuit for attentional mechanisms. *J. Neurosci.*, **26**, 7348–7361.
- Zikopoulos, B. & Barbas, H. (2010) Changes in prefrontal axons may disrupt the network in autism. *J. Neurosci.*, **30**, 14595–14609.
- Zikopoulos, B. & Barbas, H. (2013) Altered neural connectivity in excitatory and inhibitory cortical circuits in autism. *Front. Hum. Neurosci.*, **7**, 609.
- Zikopoulos, B., John, Y.J., García-Cabezas, M.A., Bunce, J.G. & Barbas, H. (2016) The intercalated nuclear complex of the primate amygdala. *Neuroscience*, **330**, 267–290.